AIChE

Modeling the Depleting Mechanism of Urea-Water-Solution Droplet for Automotive Selective Catalytic Reduction Systems

Ehab Abu-Ramadan, Kaushik Saha, and Xianguo Li
Dept. of Mechanical and Mechatronics Engineering, University of Waterloo, 200 University Avenue West, Waterloo, Ontario, Canada N2L 3G1

DOI 10.1002/aic.12523
Published online February 15, 2011 in Wiley Online Library (wileyonlinelibrary.com).

The current work aims to develop a reliable theoretical model capable of simulating the depletion process of urea-water-solution (UWS) droplets injected in a hot exhaust stream as experienced in an automotive urea-based selective catalytic reduction system. A modified multicomponent vaporization model is presented and implemented in the current study to simulate the behavior of UWS droplet in heated environment. Although water depletion is modeled as a vaporization process, urea depletion is modeled using two different approaches: (i) vaporization and (ii) direct thermal decomposition. The suitability of both depletion approaches is assessed in the current study by comparison with experimental data of the decay of a single UWS droplet in a quiescent heated environment. The decay rate of UWS droplet is accurately predicted with the multicomponent vaporization model. The possibility of internal gasification is demonstrated. Based on the complex decomposition behavior of urea, the current study proposes a decomposition mechanism for UWS droplet. The suitability of implementing the rapid mixing approach is assessed through comparison with the diffusion limit approach at various operating conditions and initial UWS droplet sizes. © 2011 American Institute of Chemical Engineers *AIChE J,* 57: 3210–3225, 2011
Keywords: urea decomposition mechanism, multicomponent droplet vaporization, internal gasification, automotive SCR system

Introduction

Automobile direct injection diesel engines are recognized for their durability, high torque density, relatively low carbon dioxide emission, and fuel economy. However, the appearance of regions of high flame temperatures during the combustion process promotes the formation of nitrogen oxides (NO_x).[1–3] Introducing new engine technologies, such as cooled exhaust gas recirculation and electronically controlled fuel injection systems, can reduce NO_x emission levels from 1000 ppm to about 200–300 ppm.[4] An efficient exhaust after treatment system is required to reach the strict NO_x regulations of 30 ppm imposed by EUVI in Europe and Tier2 Bin5 in the United States. However, the highly oxidizing environment of diesel/biodiesel engine exhausts resulting from the normal lean operating conditions presents difficulty in designing an efficient reduction mechanism. While three-way catalyst is ineffective in such oxidizing environment,[5] lean NO_x traps are limited to light duty vehicles due to durability, cost, and packaging issues.[6,7] The current preferred technology to comply with the ever-stricter NO_x emission standards of automotive diesel engines is the use of selective catalytic reduction (SCR) system with ammonia as the reducing agent.[7–12] Over a suitable catalyst, ammonia

Correspondence concerning this article should be addressed to X. Li at x6li@mecheng1.uwaterloo.ca.

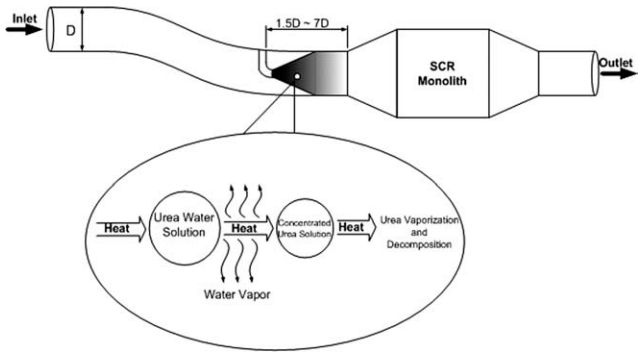

Figure 1. Schematic illustration of a typical urea-based selective catalytic reduction (SCR) after treatment system in exhaust pipe.

The magnified view shows the decomposition mechanism of a typical urea-water-solution (UWS) droplet in the exhaust pipe environment.

reduces NO to nitrogen through the standard SCR reaction mechanism[9,13]

$$4NH_3 + 4NO + O_2 \rightarrow 4N_2 + 6H_2O. \quad (R1)$$

If the exhaust gas contains equimolar amounts of NO and NO_2, NO_x reduction occurs at a faster rate through the fast SCR reaction mechanism[9,13]

$$4NH_3 + 2NO + 2NO_2 \rightarrow 4N_2 + 6H_2O. \quad (R2)$$

Difficulties associated with storage, handling, transportation, and toxic properties of ammonia prohibit its direct use in automotive applications.[4,8,14] Instead, ammonia is generated onboard using a suitable precursor. Urea is currently the preferred precursor for automotive applications because ammonia is produced directly from urea through thermal decomposition.[14] Furthermore, urea is nontoxic and commonly available.[15] To avoid the problems associated with the dosing of solid urea, a urea-water-solution (UWS), containing 32.5 wt % urea, brand name: AdBlue, is used as the reducing agent for all SCR in diesel vehicles.[12,14,15]

A basic automobile urea-based SCR system is schematically presented in Figure 1. The figure also shows the vaporization and decomposition mechanisms of a typical UWS droplet. Johnson[12] indicated that urea-based SCR is capable of achieving EPA-2010, Euro VI, and final Tier-4 emission legislations. In general, both light duty and heavy duty vehicles use the same SCR technology.[16] However, some differences concerning the dimensions and operating specifications exist. In an automobile urea-based SCR system, UWS is sprayed into the exhaust stream upstream of the SCR catalyst. Heat from the hot exhaust gas is transferred to the injected UWS droplets resulting in the generation of the reducing agent to proceed in the following steps:

1. Evaporation of the majority of water content because of its relative high volatility.[17]

$$H_2N{-}CO{-}NH_2(\text{aq. sol.}) \xrightarrow{\text{heat}} H_2N{-}CO{-}NH_2(\text{conc. sol.}) + xH_2O(g), \quad (R3)$$

2. Evaporation and decomposition of urea into ammonia and isocyanic acid.[9,17,18]

$$H_2N{-}CO{-}NH_2(\text{conc. sol.}) \xrightarrow{\text{heat}} H_2N{-}CO{-}NH_2(g) \xrightarrow{\text{heat}} NH_3(g) + HNCO(g), \quad (R4)$$

3. The hydrolysis of isocyanic acid into ammonia and carbon dioxide.[9,17,18]

$$HNCO(g) + H_2O(g) \rightarrow NH_3(g) + CO_2(g). \quad (R5)$$

The in situ-generated ammonia reduces NO_x gases into nitrogen through the standard and fast SCR $DeNO_x$ reduction mechanisms presented in reactions (R1) and (R2). In that sense, effective $DeNO_x$ reduction mechanism requires equimolar amounts of generated ammonia and NO_x. Although the introduction of insufficient amount of ammonia deteriorates the efficiency of the SCR system,[19] ammonia slip is expected if the molar ratio of ammonia to NO_x exceeds one.[9] The main design criterion for an efficient urea-based SCR system is to ensure the injection of sufficient amount of UWS capable of generating the required amount of ammonia.

In automotive applications, the continuous variations in load and engine speed combined with spatial limitations add to the complexity of the requirements of an efficient urea-SCR system. Variations in load and engine speed alter the exhaust gas temperature and space velocity, which subsequently affect the decomposition efficiency of UWS droplets. Although water vaporization rate is directly related to the exhaust temperature, urea thermolysis exhibits a very complex temperature dependent pathway.[19,20] Heating urea to temperatures above 573 K can result in the consumption of a considerable amount of the generated ammonia and isocyanic acid to produce melamine complexes,[19,20] which degrade the structural and thermal properties of the catalyst surface. Automotive spatial restrictions can result in incomplete decomposition of UWS and/or inhomogeneous distribution of reductant and exhaust gaseous mixture at the entrance of the catalyst. The residence time between the injection of UWS and the catalyst entrance for a typical automotive SCR system is less than 0.1 s. By measuring the relative amounts of urea, ammonia, and isocyanic acid at the catalyst entrance in a typical SCR system with urea residence time around 0.09 s, Koebel et al.[9] reported that ammonia conversion efficiency increases from 15% to only 50% as the exhaust gas temperature increases from 528 to 713 K.

Improving the $DeNO_x$ efficiency of an automotive urea-SCR system requires: (i) maximizing the evaporation and decomposition efficiency of UWS droplets, (ii) efficient control system to maintain a mean equimolar ratio between the generated ammonia and NO_x at varying operating conditions, and (iii) optimized injection system to minimize wall deposition while providing uniform distribution of exhaust gases and reductant mixture at the entrance of the catalyst. Numerical modeling can provide major contribution toward the development of highly efficient urea-SCR system. Reliable computational model can be implemented to test various design features at relatively low financial and time costs.

Furthermore, a reliable computational model complements experimental investigations by providing detailed flow and thermal analysis. Developing a reliable numerical model for the UWS injection system and decomposition process is a complex task because it needs to accurately represent the atomization process of the injected liquid jet, the vaporization and thermolysis processes of UWS droplets in the heated exhaust gas environment, and spray/wall interaction. Although standard atomization and spray/wall interaction models can be implemented,[21] the complexity of the vaporization and thermolysis processes of UWS prohibits the direct application of standard depletion models. The developed numerical model should estimate accurately the duration of the depletion of UWS droplet under different operating conditions because of the short residence time in automotive SCR systems. In that sense, precise mathematical description of the depleting mechanism of UWS droplet is the foundation for developing a numerical model capable of representing an automotive urea-based SCR system.

Various techniques have been proposed to model the UWS decomposition process. The simplest model estimates the gas concentration of ammonia, isocyanic acid, and water vapor at the catalyst entrance through an experimentally determined efficiency conversion factor.[22] Although the conversion efficiency factor model accounts for the temperature and flow rates of both the exhaust gaseous and UWS, it cannot estimate the reducing gas spatial distribution at the catalyst entrance. The conversion factor model does not provide enough information about UWS spray and decomposition processes to optimize the UWS dosing system, because it neglects the effects of UWS injection angle and location on ammonia conversion efficiency and the uniformity of the concentration distribution at the catalyst entrance. For design optimization purposes, Chen and Williams[23] proposed the use of Eddy-dissipation model to simulate urea thermolysis. However, neglecting of chemical kinetic data may lead to ambiguous results. The mechanism for urea thermolysis is strongly dependent on the exhaust gas temperature. Urea droplets are required to heat up to a critical temperature, $T_l \geq 425$ K, before effective thermolysis occurs.[20] This criterion of critical temperature and also the water vaporization process seem to be missing in the model proposed by Chen and Williams.[23]

As UWS droplet is essentially a bi-component mixture, some researchers suggested to divide the decomposition process of UWS droplet into two consecutive stages; (i) complete evaporation of water followed by (ii) urea depletion through vaporization and/or decomposition.[21,24–29] Although the vaporization process of water content can be modeled using a well-established vaporization model,[30,31] the depletion of urea requires the development and implementation of special model. Ström et al.[21] proposed to model urea depletion as a heat transfer limited process at a constant temperature of 425 K. This model assumes that after the water content is completely evaporated, pure solid urea droplets are heated to a temperature of 425 K with no mass exchange with the gas phase. Once the droplet reaches 425 K, all of the convective heat transferred from the surrounding gas phase to the droplet surface is used to vaporize urea with no sensible heat change in the droplet. However, urea can be heated to temperatures higher than the critical temperature of 425 K assumed by Ström et al.[21] as observed experimentally by Lundström et al.[32] In particular, all of the differential scanning calorimeter curves presented in Ref. 32 showed continuous fluctuations in the heat flux of a 32.5 wt % UWS for temperatures lower than 573 K. These fluctuations indicate phase changes and are expected to cease once the sample reaches its thermal equilibrium. The conditions for thermal equilibrium should be calculated rather than being imposed for accurate estimate of the depletion duration.

Two other computational models describing the depletion process of urea were proposed by Birkhold et al.[25,26] After the complete evaporation of water, urea depletion was modeled either as an evaporation process with an experimentally determined saturation pressure curve,[25] or with an extended Arrhenius expression.[26] On comparison with the experimental measurements of Kim et al.,[24] both models overpredicted the calculated conversion to ammonia at relatively high gas temperatures, $T_\infty = 673$ K. The reason for deviation could be associated with the overestimation of saturation pressure and the kinetic parameters. Comparison with urea saturation pressure correlation measured by Emel'yanenko et al.[33] confirms that Birkhold et al.[25] overestimated urea saturation pressure. Although the use of a chemical kinetic model is required to estimate the effect of temperature on urea thermolysis, accurate parameters and reaction mechanisms are necessary for reliable simulations. Based on the observation that gaseous urea is unstable at elevated temperatures, Birkhold et al.[26] concluded that the evaporated urea decomposes immediately into ammonia and isocyanic acid. The intermediate vaporization step in Reaction (R4) was neglected, and urea thermolysis was modeled directly from solid/molten urea to ammonia and isocyanic acid.[26] In that sense, Birkhold et al.[26] used a seemingly appropriate reduced reaction mechanism with reaction enthalpy equals to the vaporization and decomposition enthalpies. The reduced reaction mechanism implemented by Birkhold et al.[26] is an improvement over the oversimplified reduced reaction mechanism used by Yi.[27] The hydrolysis of isocyanic acid was modeled in Ref. 26 as a subsequent reaction. Modeling reactions (R4) and (R5) individually is valid throughout the SCR system. However, comparison with the kinetic parameters measured from the experimental data of Yim et al.[18] shows that Birkhold et al.[26] overestimated the activation energy. Overestimating the activation energy leads to an overestimation of the droplet temperatures and, consequently, the decay rate.[34] Munnannur and Liu[28,29] improved the predictability of Birkhold et al.[26] model by using different kinetic parameters.

The exact water content in the UWS droplet at the start of effective decomposition of urea is not exactly known. The water evaporation process leads to a spatial urea concentration gradient with a maximum at the droplet surface. As water continues to evaporate, urea concentration at the surface increases until a urea shell is formed at the droplet surface. The shell is expected to form before the droplet reaches the boiling temperature of water as experimentally demonstrated by Wang et al.[35] The trapping of higher volatile components inside the droplet interior is well-established phenomenon both numerically and experimentally.[36,37] It should be noted that Ström et al.[21] and Birkhold et al.[25,26] assumed that UWS droplet remains at the standard saturation temperature of 373 K until the droplet water content

vanishes to handle the trapped water inside a heated UWS droplet. Such assumption violates the boiling point elevation phenomenon. In particular, Sirignano and Wu[38] demonstrated that the effective boiling point of individual droplet components in a multicomponent droplet is exponentially correlated with its local concentration. In that sense, as water evaporates from UWS due to droplet heating, water concentration in the droplet decreases, which results in an exponential increase in the effective boiling point of water beyond 373 K. Violating the boiling point elevation phenomenon will affect the calculated depletion time, and consequently the design of the SCR system. The exact water content at various stages of the UWS droplet decomposition/vaporization process can be predicted using a validated multicomponent vaporization model instead of separating the decomposition process into two distinct and consecutive processes.

Developing a reliable mathematical model describing the depletion mechanism of a typical UWS droplet for automotive SCR De-NO_x systems is the main objective of the current work. As indicated from the analysis of the reviewed literature, achieving this objective requires the implementation of: (i) a validated multicomponent droplet vaporization model with separate depletion law for each component, (ii) urea decomposition mechanism that is suitable for automotive SCR system, and (iii) reliable material data of the involved species. A modified version of the recently proposed semianalytical model for multicomponent droplet vaporization of Saha et al. (submitted) is presented in details in the model formulation section to describe the behavior of UWS droplet in a heated environment. Although water vaporization rate is calculated using the saturation pressure correlation presented in Saha et al., submitted, urea depletion is modeled either as a vaporization process or a direct thermolysis process from molten urea to ammonia and isocyanic acid. The presented mathematical model accounts for the temporal variations of the material properties, and more importantly the inequalities in the gas phase diffusivity. The validity of the developed model and the implemented material and transport properties are assessed in the results and discussion section through comparison with experimental data of the decay rate of an individual UWS droplet in heated environment to exclude the interactions among droplets and turbulence effects. The presented theoretical investigation aims to provide an understanding of the complicated urea decomposition mechanism, which is essential for the design of an efficient urea-based SCR DeNO_x system.

Model Formulation

Physical description and assumptions

Theoretical description of the behavior of a spherically symmetric UWS droplet in a stagnant heated environment is presented in this section. The presented theoretical model combines the simplicity of Sirignano's model[39] and the accuracy of the model developed by Renksizbulut et al.[40] Maintaining the spherical symmetry of the droplet reduces the mathematical model to a one dimensional transient problem. Initially, the UWS droplet is characterized by a specified initial diameter, and uniform distribution of temperature and species, such that

$$d(t=0)=d_0,\quad T_l(r,t=0)=T_{l,0}\qquad \text{and}$$
$$Y_{i,l}(r,t=0)=Y_{i,l,0}. \quad (1)$$

The heated environment is represented by a hot gas mixture with uniform temperature, pressure, and species of T_∞, P_∞, and $Y_{i,\infty}$, respectively. Physically, the heat transported from the hot environment to the droplet is used to heat the droplet and deplete its components. In addition to spherical symmetry, the outlined mathematical model is based on the following assumptions:

1. The gas phase surrounding the droplet is in a quasi-steady state because the thermal diffusivity of the gas phase is much higher than that of the liquid phase,
2. the surrounding gas mixture is insoluble in the liquid droplet, which leads to one-way diffusion, or the so-called Stefan flow,
3. both liquid and gaseous phase at the droplet surface are at thermodynamic equilibrium,
4. secondary effects such as Soret and Dufour effects and pressure diffusion are negligible, and
5. the formation of biuret and high molecular complexes are neglected.

Multicomponent Vaporization Mechanism

Gas phase analysis

The evaporation process of a multicomponent droplet containing n vaporizing components into the hot exhaust gas mixture is described in this section. Analyzing the heat and mass transfer processes in the gas phase near the droplet surfaces determines the amount of heat transferred to the droplet liquid phase and the instantaneous vaporization rate of any of the droplet vaporizing component. The heat transferred from the gas phase to the droplet surface is consumed by droplet heating and phase change. This physical behavior is expressed using the energy conservation at the droplet surface, such that

$$\dot{Q}_{g,s}+\dot{Q}_{\text{rad}}=\dot{Q}_{l,s}+\sum_{i=1}^{n}\dot{m}_i L_{\text{vap},i}. \quad (2)$$

The convective heat transfer rate to the droplet surface is expressed in terms of heat transfer coefficient, $h_{g,s}$, which is nondimensionalized by the surrounding gaseous film Nusselt number, $Nu_{g,s}$, as follows

$$\dot{Q}_{g,s}=\pi d^2 h_{g,s}\left(T_\infty-T_{l,s}\right)=\pi d Nu_{g,s}k_{g,s}\left(T_\infty-T_{l,s}\right). \quad (3)$$

The rate of radiation heat transfer transferred to the droplet from the exhaust walls is computed from

$$\dot{Q}_{\text{rad}}=\pi d^2\sigma\varepsilon\left(T_{\text{wall}}^4-T_{l,s}^4\right). \quad (4)$$

The contribution of radiation heat transfer is included here to make the model general, and it is important in the automotive exhaust SCR systems. The sensible heat transferred to the droplet surface is

$$\dot{Q}_{l,s}=m_l Cp_l\frac{\partial T_{l,s}}{\partial t}. \quad (5)$$

Conservation of vaporizing species across the droplet surface is implemented to evaluate the evaporation rate of vaporizing components. Assuming the evaporation process to be quasi-steady, the species conservation equation is expressed as

$$\dot{m}_i = Y_{i,g,s}\sum_{j=1}^{n}\dot{m}_j + j_{i,g,s}. \tag{6}$$

As the only species crossing the droplet surface are the liquid droplet vaporizing components, the total evaporating mass flow rate from the droplet surface becomes

$$\dot{m} = \sum_{i=1}^{n}\dot{m}_i = \frac{\sum_{i=1}^{n} j_{i,g,s}}{1-\sum_{i=1}^{n} Y_{i,g,s}}. \tag{7}$$

The mass diffusion of specie i is expressed in terms of mass transfer coefficient, $h_{m,i}$, which is nondimensionalized by the surrounding gaseous Sherwood number, $Sh_{i,g,s}$, as follows

$$j_{i,g,s} = \pi d^2 h_{m,i}\left(Y_{i,g,s} - Y_{i,\infty}\right) = \pi d\bar{\rho}_{g,s}\Gamma_{i,g,s}Sh_{i,g,s}\left(Y_{i,g,s} - Y_{i,\infty}\right). \tag{8}$$

Gaseous-liquid interface analysis

The subscript g,s denotes the gaseous film surrounding the droplet. In this region, both liquid and gaseous phase at the droplet surface are at thermodynamic equilibrium. Hence, the vapor fraction of the evaporating species at the droplet surface can be determined from Raoult's law, such that

$$X_{i,s} = X_{i,l,s}\frac{P_{\text{sat}}\left(T_{l,s}\right)}{P_\infty}; \qquad Y_{i,s} = \frac{x_{i,s}\text{MW}_i}{\sum_{j=1}^{N} X_{j,s}\text{MW}_j}. \tag{9}$$

The physical properties of the surrounding film is evaluated using the 1/3 rule, such that

$$T_{g,s} = T_{l,s} + \frac{1}{3}\left(T_\infty - T_{l,s}\right) \text{ and } Y_{i,g,s} = Y_{l,s} + \frac{1}{3}\left(Y_{i,\infty} - Y_{i,s}\right). \tag{10}$$

The surrounding gaseous film Nusselt number, $Nu_{g,s}$, and the vaporizing component Sherwood number, $Sh_{i,g,s}$, are expressed as

$$Nu_{g,s} = \frac{Nu_0}{F_T}; \quad Sh_{i,g,s} = \frac{Sh_{i,0}}{F_M}. \tag{11}$$

where Nu_0 and $Sh_{i,0}$ are evaluated by the well-known correlations of Clift et al.,[41] which is valid for $Re_l < 400$

$$Nu_0 = 1 + \left(1 + Re_l Pr\right)^{1/3}\max\left[1, Re_l^{0.077}\right], \tag{12a}$$

$$Sh_{i,0} = 1 + \left(1 + Re_l Sc_{i,g,s}\right)^{1/3}\max\left[1, Re_l^{0.077}\right], \tag{12b}$$

where $\text{Re}_l = v_{\text{rel}}d/\upsilon_{g,s}$ is zero in the current analysis because $v_{\text{rel}} = 0$. The correction factors, F_M and F_T can be estimated using the empirical correlation[42]

$$F_T = \left(1 + B_T\right)^{0.7}, \quad F_M = \left(1 + B_M\right)^{0.7} \tag{13}$$

where B_T and B_M are the heat transfer and global mass transfer numbers

$$B_T = \frac{\left(\sum_{i=1}^{n}\dot{m}_i Cp_{i,g,s}\right)\left(T_\infty - T_{l,s}\right)}{\sum_{i=1}^{n}\dot{m}_i L_{\text{vap},i} + \dot{Q}_{l,s} - \dot{Q}_{\text{rad}}}, \tag{14a}$$

$$B_M = \frac{\sum_{i=1}^{n} Y_{i,g,s} - \sum_{i=1}^{n} Y_{i,\infty}}{1 - \sum_{i=1}^{n} Y_{i,g,s}}, \tag{14b}$$

It should be noted that the logarithmic term appearing in most of the droplet vaporization modeling papers cancels out on implementation (see, e.g., Eqs. 8, 10, and 17 in Ref. 30).

Liquid phase analysis

The instantaneous distribution of temperature and species concentrations inside the UWS droplet falls between the limiting ranges of rapid mixing (RM) and diffusion limit (DL) models. Both models are presented in this section.

RM model

The RM model postulates infinitely high diffusivities for the liquid phase. This results in spatially uniform and temporally varying temperature and species concentration distribution in the droplet. In that sense, $T_l\ (r,t) = T_{l,s}\ (t)$ and $Y_{i,l}\ (r,t) = Y_{i,l,s}\ (t)$. Temporal variation of the droplet temperature is evaluated by using the energy balance at the droplet surface as described by Eq. 5. Temporal variations of vaporizing species concentrations are evaluated using the conservation of vaporizing species across the droplet surface as described by Eq. 6. If urea is assumed to be decomposing directly from the liquid phase to gaseous ammonia and isocyanic acid, both Eqs. 6 and 22 or 23 will be used simultaneously to evaluate the decay rate of the UWS droplet.

DL model

The roles of the thermal and interspecies liquid diffusivities are considered in the DL model. The greater the interspecies liquid diffusivity of the component in a multicomponent droplet, the faster it diffuses to the droplet surface. The governing equations in dimensional forms for DL approach for energy and species in the droplet liquid phase in terms of moving boundary of the droplet are

$$\frac{\partial T_l}{\partial t} - \frac{r}{r_s}\dot{r}_s\frac{\partial T_l}{\partial r} = \frac{\alpha_l}{r^2}\frac{\partial}{\partial r}\left(r^2\frac{\partial T_l}{\partial r}\right), \tag{15}$$

and

$$\frac{\partial Y_{i,l}}{\partial t} - \frac{r}{r_s}\dot{r}_s\frac{\partial Y_{i,l}}{\partial r} = \frac{\Gamma_{i,l}}{r^2}\frac{\partial}{\partial r}\left(r^2\frac{\partial Y_{i,l}}{\partial r}\right), \tag{16}$$

with the following boundary conditions at the droplet center

$$\frac{\partial T_l(r=0)}{\partial r} = 0, \text{ and } \frac{\partial Y_{i,l}(r=0)}{\partial r} = 0 \tag{17}$$

At the droplet surface, the energy balance and the species conservation are used to obtain

$$\frac{\partial T_l(r=r_s)}{\partial r} = \frac{1}{\pi d^2 k_l}\dot{Q}_{l,s}, \tag{18a}$$

and

$$\frac{\partial Y_{i,l}(r=r_s)}{\partial r} = \frac{1}{\pi d^2\rho_l\Gamma_{i,l}}\left(Y_{i,s}\sum_{j=1}^{n}\dot{m}_j - \dot{m}_i\right). \tag{18b}$$

The DL model presented here accounts for property variations with temperature in the liquid phase by updating the transport properties of the droplet at each time step.

Mathematical modeling of urea depletion

In the current study, urea depletion from the UWS droplet is modeled either as a vaporization process or a direct thermolysis process from molten urea to ammonia and isocyanic acid. Mathematical descriptions of both depletion techniques are presented here.

Vaporization approach

The presented multicomponent droplet vaporization model is used to model urea evaporation process. Urea latent heat of vaporization is computed from the steady-flow form of the first law of thermodynamics, such that

$$L_{\mathrm{vap},u}(T_{l,s}) = L_{\mathrm{vap},u}(T_{\mathrm{std}}) + \int_{T_{\mathrm{std}}}^{T_{l,s}} Cp_{u(g)}dT - \int_{T_{\mathrm{std}}}^{T_{l,s}} Cp_{u(l)}dT, \tag{19}$$

where $L_{\mathrm{vap},u}$ (T_{std} = 298K) = 1.4553 × 10^3 KJ/kg. The correlations for gaseous and liquid urea specific heat will be discussed in the material properties section. The vaporized urea is then thermally decomposed into ammonia and isocyanic acid. As the decay rate of urea is modeled as an evaporation process, this approach will be referred to as "Vap."

Direct thermolysis approach

The second technique models urea depletion as a thermal decomposition directly from molten urea to gaseous ammonia and isocyanic acid. In this case, the phase change of urea is neglected. This technique is based on the observation that urea does not seem to be stable in the gaseous phase. Based on the thermal gravimetric analysis (TGA), Schaber et al.[20] reported that heating urea to temperatures higher than 425 K results in rapid mass decay of urea sample. The mass decay is associated mainly with the release of ammonia and isocyanic acid as indicated by the Fourier transform-infrared (FTIR) analysis.[20] In that sense, it can be assumed that urea decomposition rate is much faster than urea vaporization rate, and both vaporization and decomposition can be reduced to one reaction mechanism.

In the direct decomposition approach, the energy transferred to the UWS droplet surface is calculated from

$$\dot{Q}_{g,s} + \dot{Q}_{\mathrm{rad}} = \dot{Q}_{l,s} + \dot{m}_w L_{\mathrm{vap},w} + \dot{m}_u H_{\mathrm{th},u(l)}. \tag{20}$$

where

$$H_{th,u(l)}(T_l) = H_{\mathrm{th},u(l)}(T_{\mathrm{std}}) + \int_{T_{\mathrm{std}}}^{T_g} Cp_{\mathrm{NH_3}(g)}dT + \int_{T_{\mathrm{std}}}^{T_l} Cp_{\mathrm{HNCO}(g)}dT - \int_{T_{\mathrm{std}}}^{T_{l,s}} Cp_{u(l)}dT, \tag{21}$$

and $H_{\mathrm{th},u(l)}(T_{\mathrm{std}} = 298\mathrm{K}) = 3.0888 \times 10^3$ kJ/kg. It should be noted that Eq. 20 can be reduced to Eq. 2 by replacing $H_{\mathrm{th},u(l)}$ with $L_{\mathrm{vap},u}$. $\dot{Q}_{g,s}$, $\dot{Q}_{\mathrm{rad}}$, and $\dot{Q}_{l,s}$ are evaluated from Eqs. 3–5, respectively. Although the species conservation equation is applied to calculate $\dot{m}_w$, the decomposition rate of urea is calculated by using a kinetic model similar to the one originally developed for thermolysis of pulverized coal particles,[43] such that

$$\dot{m}_u = -A_{\mathrm{th}} \exp\left(\frac{-E_{\mathrm{th}}}{R\bar{T}_l}\right) \bar{Y}_{u,l} m_l, \tag{22}$$

It can be argued that because urea vapor is a prerequisite for the decomposition to occur, the decomposition takes place only at the boundary layer region of the droplet. The decay rate of urea may be better presented using a surface expression rather than the volumetric expression described by Eq. 22. A modified version of the surface decay rate of urea originally developed by Birkhold et al.[26] is presented in the current study to account for the presence of water in the boundary layer of the droplet. The modified expression is

$$\dot{m}_u = -A_{\mathrm{th},s} \exp\left(\frac{-E_{\mathrm{th},s}}{RT_{l,s}}\right) Y_{u,s}\left(2\pi r_s^2\right), \tag{23}$$

For comparison purposes, both expressions will be used in the current study. Although urea depletion rate obtained from the volumetric expression, Eq. 22, will be referred to as "Kinetics-V," urea depletion rate obtained from the surface expression, Eq. 23, will be referred to as "Kinetics-S". However, one has to be careful in the selection of the kinetic parameters. The decomposition parameters must be based on the volumetric reaction of liquid urea for Eq. 22 and surface reactions for Eq. 23 because A_{th} and $A_{th,s}$ have different units.

Once the decay rate of urea is determined through either Eq. 22 or 23, the production rates of ammonia and isocyanic acid can be obtained from

$$\dot{m}_{\mathrm{NH_3}} = -\frac{\mathrm{MW_{NH_3}}}{\mathrm{MW}_u}\dot{m}_u, \quad \dot{m}_{\mathrm{HNCO}} = -\frac{\mathrm{MW_{HNCO}}}{\mathrm{MW}_u}\dot{m}_u. \tag{24}$$

This expression is deduced from the fact that 1 mol of thermally decomposed urea produces 1 mol each of ammonia and isocyanic acid.

Material and Transport Properties

All the properties of the individual components of both liquid and gaseous materials are temperature dependent. Aside from urea, temperature-dependent properties for all materials are readily available in the literature Saha et al., submitted. For the properties of gaseous urea, no experimentally validated correlation or tabulated data could be located. The reason could be the instability of urea in the gaseous phase as discussed. Due to the lack of experimental data, the kinetic theory is implemented to determine the viscosity, thermal conductivity, and diffusivity. A correlation for the specific heat of gaseous urea is extracted from the tabulated data in Fluent 6.3.2 package.[45] Although the experimental source for the extracted specific heat could not be located. The extracted correlation for the specific heat of gaseous urea is implemented in the in-house built code for the depletion of UWS droplet. Reliable values for the specific heat of gaseous urea could not be found in the literature. The reason could be the difficulties associated with accurately measuring the properties of gaseous urea due to the instability of urea in the gas phase. In that sense, it is proposed to simply use a constant value for urea latent heat of vaporization. As urea decomposes immediately into ammonia and isocyanic acid, the energy balance will not be affected. The results from this approach will be labeled as "Vap1," and the results obtained

Table 1. Kinetic Parameters of the Reaction Rate Constants for Urea Thermolysis Used in This Study

Model	Kinetics-V1	Kinetics-V2	Kinetics-V3	Kinetics-S
Based on	Yim et al.[18]	Aoki et al.[49]	Schaber et al.[20]	Birkhold et al.[28]
$A_{th}/A_{th,s}$	4855.1 s^{-1}	12676 s^{-1}	48595.2 s^{-1}	0.42 kg/s m
$E_{th}/E_{th,s}$	2.3×10^4 J/mol	6.5×10^4 J/mol	6.6×10^4 J/mol	6.9×10^4 J/mol

with the varying latent heat of vaporization will be labeled as "Vap2."

For liquid urea, the specific heat correlation is extracted from the tabulated data.[46] Other material properties, including density, viscosity, and thermal conductivity are extracted from the AdBlue manufacturer's specifications.[47] For the liquid phase analysis, the most significant parameter is the species diffusivity of urea in water. The variation of binary species diffusivity of urea in water used in the current study was obtained from the experimental findings of Longsworth.[48]

The saturation vapor pressure of urea is required if the vaporization approach is implemented. The vapor pressure of urea was measured by Emel'yanenko et al.[33] However, the measurements were limited to the range $T_u \in$ [358K, 376.5K]. Instead of extrapolating the empirical correlation of Emel'yanenko et al.,[33] Clausius–Clapeyron equation is implemented, such that

$$P_{\mathrm{sat},u}(T_{l,s}) = P_{\mathrm{sat,ref}}(T_{\mathrm{ref}}) \exp\left(\int_{T_{\mathrm{ref}}}^{T_{l,s}} \frac{L_{\mathrm{vap},u}}{\mathrm{RT}} dT\right), \qquad (25)$$

where $P_{\mathrm{sat,ref}}(T_{\mathrm{ref}} = 376.5\mathrm{K}) = 2.96\mathrm{Pa}$ as measured by Emel'yanenko et al.[33]

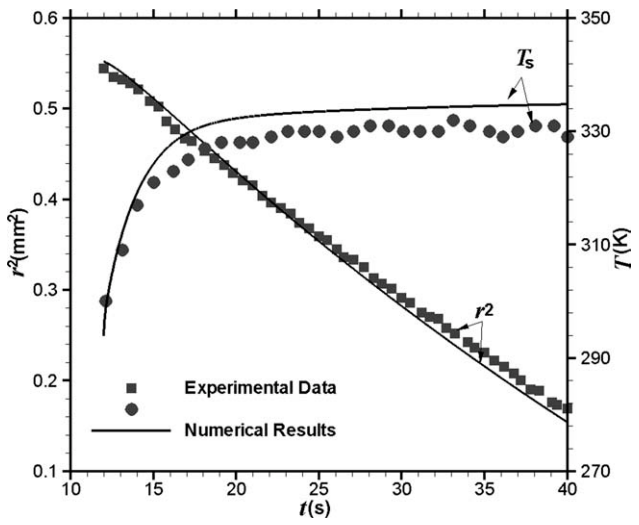

Figure 2. Comparison between the experimental data of Daif et al.[50] and the present numerical predictions for the time evolution of the surface temperature, T_s, and size, r^2, of a fuel mixture droplet (25% heptanes and 75% decane).

The ambient and initial conditions are: $T_\infty = 348$ K, $P_\infty = 1$ atm, $U_\infty = 3.1$ m/s, $T_{d,0} = 294$ K, and $r_{d,0} = 0.743$ mm.

Table 2. Physical Properties for the Gaseous and Liquid Mixtures Used in This Study

	Gaseous mixture	Droplet mixture
Density	$\rho_g = \frac{P_g}{RT_g \sum_{i=1}^{N} \frac{Y_{i,g}}{MWi}}$	$\rho_l = \frac{1}{\sum_{i=1}^{n} \frac{Y_{i,l}}{\rho_{i,l}}}$
Thermal conductivity	$k_g = \sum_{i=1}^{N} \frac{Xi,gk_{i,g}}{\sum_j X_{j,g}\varphi_{ij}}$	$k_l = \sum_{i=1}^{n} Y_{i,l}k_{i,l}$
Specific heat	$Cp_g = \sum_{i=1}^{N} Y_{i,g}Cp_{i,g}$	$Cp_l = \sum_{i=1}^{n} Y_{i,l}Cp_{i,l}$
Viscosity	$\mu_g = \sum_{i=1}^{N} \frac{Xi,g\mu_{i,g}}{\sum_j X_{j,g}\varphi_{ij}}$	$\mu_l = \sum_{i=1}^{n} Y_{i,l}\mu_{i,l}$
Diffusion coefficient	$\Gamma_{i,g} = \Gamma_{i,\mathrm{air}}(T_g)$	Longsworth[49]

The current study models the direct thermal decomposition of urea using either a volumetric model described by Eq. 22 and referred to as Kinetics-V or a surface model described by Eq. 23 and referred to as Kinetics-S. In addition to the kinetic models, these approaches differ in the values of the kinetic parameters for urea decomposition. The decomposition parameters must be based on the volumetric reaction of liquid urea for Eq. 21 and surface reactions for Eq. 22 because A_{th} and $A_{th,s}$ have different units. Table 1 presents the volumetric kinetic parameters extracted from the experimental results of urea decomposition by Yim et al.,[18] indicated by Kinetics-V1, and Aoki et al.,[49] indicated by Kinetics-V2. As the volumetric reaction occurs at the droplet level, the kinetic parameters should be based on the decomposition rate of molten urea rather than urea concentration. The authors extracted the kinetic parameters for urea decomposition from the experimental decay rate of urea sample, which was presented in Figure 2 in Ref. 20. The extracted parameters are also presented in Table 1, and referred to as Kinetics-V3. The parameters for Kinetic-S were deduced by Birkhold et al.[26] No other parameters for Kintics-S could be found in the literature.

The evaporation and decomposition processes of UWS droplets alter the thermophysical properties of the gaseous and liquid mixtures. Correlations used for the calculations of thermophysical properties of the gaseous and liquid phase mixtures are presented in Table 2. The parameter φ_{ij} is calculated from

$$\varphi_{ij} = \frac{\left[1 + \left(\frac{\theta_i}{\theta_j}\right)^{1/2} \left(\frac{\mathrm{MW}_i}{\mathrm{MW}_j}\right)^{1/4}\right]^2}{\left[8\left(1 + \frac{\mathrm{MW}_i}{\mathrm{MW}_j}\right)\right]^{1/2}}. \qquad (26)$$

where θ_i is the individual species property of the mixture property being calculated.

Solution Procedure

The temporal and spatial evolutions of species and temperature distributions within the droplet are evaluated in the current study using two Matlab codes developed in-house: one for the vaporization approach, and another for the direct thermolysis approach. The solution procedure adopted in this study is presented below:

Outline for the vaporization approach

1. Use $Y_{i,l,s}$ and $T_{l,s}$ from the initial conditions or the results of previous time step to determine the gaseous film composition and temperature through Eqs. 9 and 10;

2. Use $Y_{i,g,s}$ and $T_{g,s}$ to calculate the physical properties of the gaseous film mixture as outlined in Table 2, and the dimensionless parameters, Nu_0 and $Sh_{i,g,s}$;

3. Calculate $\dot{m}$ from Eq. 7;

4. Use the calculated $\dot{m}$ to calculate $\dot{m}_i$ from Eq. 6;

5. Apply an iterative procedure to calculate $\dot{Q}_{g,s}$ from Eq. 3, $\dot{Q}_{\text{rad}}$ from Eq. 4, and $\dot{Q}_{l,s}$ from Eq. 2 with B_T acting as the control parameters;

6. For the RM model, a numerical time integration scheme is applied to solve Eq. 2 and (3) to update the droplet temperature and composition at each time step;

7. For the DL model, the results from steps (1)–(5) are used as the boundary conditions at the droplet surface as described by Eq. 18. The governing equations for the DL model are nondimensionalized and discretized using the time implicit finite difference method. The nondimensional equations are presented in Appendix A.

Outline for the direct thermolysis approach

Applying the direct thermolysis technique reduces the multicomponent droplet vaporization model to a single component model. A similar outline to the one presented above is implemented here with the following modifications;

1. Omit step 3;

2. Calculate $\dot{m}_w$ from Eq. 6,

3. For Kinetics-V, calculate $\dot{m}_u$ from Eq. 22 if $\overline{T_l} \geq$ 425K,

4. For Kinetics-S, calculate $\dot{m}_u$ from Eq. 23 if $T_{l,s} \geq$ 425K.

Results and Discussion

Algorithm validation

The validity of the proposed multicomponent vaporization model is established by comparing its predictions to benchmark experimental data. Figure 2 shows a comparison between the experimentally measured data of Ref. [50] and the predictions of the multicomponent vaporization model presented in the current study for the vaporization behavior of a suspended 25% heptane and 75% decane (volume percentage) droplet subject to the conditions of $T_\infty = 348$ K, $P_\infty = 1$ atm, and $U_\infty = 3.1$ m/s. The droplet initial conditions are $T_{d,0} = 294$ K and $r_{d,0} = 0.743$ mm. The experimental investigations were conducted in a thermal wind-tunnel fitted with a video recording system and an infrared camera to monitor the changes in the size and temperature of an individually suspended multicomponent droplet in forced convection environment. The numerical predictions are obtained using the DL approach. Figure 2 demonstrates that the multicomponent vaporization model is capable of accurately predicting the temporal evolution of the radius and surface temperature of the multicomponent droplet. The maximum relative errors for radius and temperature predictions are -4.43% and $+1.75\%$, respectively. The multicomponent vaporization model is thus validated. It will be applied in the current study to analyze the vaporization behavior UWS droplet at various operating conditions.

Depletion model assessment

The suitability of the urea depletion modeling technique and properties is assessed through comparison with experimental data of the decay rate of an individual UWS droplet in heated environment to exclude the interactions among droplets and turbulence effects. Recently, Wang et al.[35] recorded the temporal change of the size of a suspended UWS droplet in a heated chamber using a high-speed charge-coupled device (CCD) camera. Radiation effects were minimized in the experimental study of Wang et al.,[35] by the use of radiative shields. Comparison between the experimentally extracted data of Wang et al.[35] and the numerical predictions of the current study for the temporal reduction of the diameter of a UWS droplet in a quiescent-heated environment is presented in Figure 3. The numerical predictions are obtained using the DL approach. To imitate the experimental conditions, radiation heat transfer is neglected in the

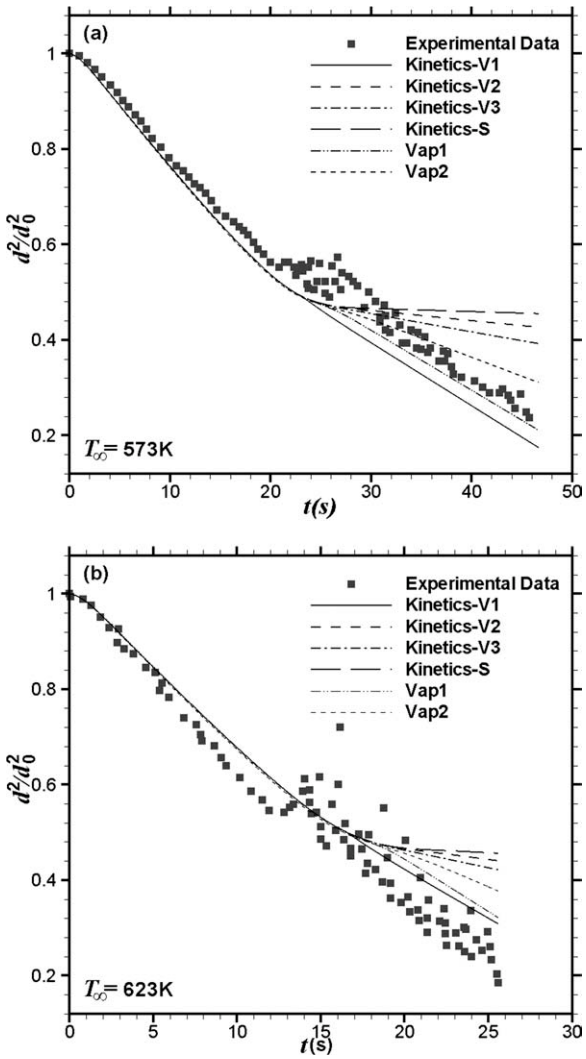

Figure 3. Comparison between the experimental data of Wang et al.[35] and the present numerical predictions for the temporal evolution of a UWS droplet size, d^2/d_0^2, under the following conditions: (a) $T_\infty = 573$ K, $P_\infty = 1$ atm, $Y_{u,\infty} = Y_{w,\infty} = 0$, $T_{l,0} = 300$ K, $d_0 = 0.920$ mm, and $Y_{u,0} = 0.325$; and (b) $T_\infty = 623$ K, $P_\infty = 1$ atm, $Y_{u,\infty} = Y_{w,\infty} = 0$, $T_{l,0} = 300$ K, $d_0 = 0.869$ mm, and $Y_{u,0} = 0.325$.

model calculations. The ambient and initial droplet conditions are; $T_\infty = 573$ K, $P_\infty = 1$ atm, $Y_{u,\infty} = Y_{w,\infty} = 0$, $T_{l,0} = 300$ K, $d_0 = 0.920$ mm, $Y_{u,0} = 0.325$ in Figure 3a, and $T_\infty = 623$ K, $P_\infty = 1$ atm, $Y_{u,\infty} = Y_{w,\infty} = 0$, $T_{l,0} = 300$ K, $d_0 = 0.869$ mm, $Y_{u,0} = 0.325$ in Figure 3b.

Figure 3 demonstrates that the numerically predicted and experimentally extracted time evolution of the size of a UWS droplet exposed to hot ambient conditions can be divided into two stages resembling a batch distillation process governed by volatility differentials. In that sense, droplet components vaporize in sequence starting from the components with higher vapor pressure. For a UWS droplet, water is expected to vaporize first, because it is the component with the higher vapor pressure. This is affirmed by the coincidence of all the numerical results during the first stage of droplet depletion because the modeling of water vaporization is the same for all numerical approaches. Qualitatively and quantitatively, the numerical results match the experimental data over the first depleting stage very well for both ambient conditions as illustrated in Figures 3a and 3b. However, a small deviation is observed in the duration and the rate of droplet depletion of the first stage. In particular, the numerical results overestimate the duration of the first decomposition stage by about 5 and 11% for the conditions in Figures 3a and 3b, respectively. Such deviations are accepted given the relatively large initial droplet sizes. As the depletion of water is governed by the well-known d^2 law, the quantitative deviation is expected to be reduced by 100 times for the practical Sauter mean diameter (SMD) of a UWS droplet.

Although the numerical results overestimate the droplet decay rate for the conditions in Figure 3a, an underestimate of the droplet decay rate is observed in Figure 3b. The deviation can be attributed to the uncertainty associated with the diffusivity of urea in liquid water and the inherent errors in the experimental data measured from the CCD camera. In the absence of internal circulation, vaporization is governed by the volatility of individual components and the rate of species diffusion. Water vaporization from the droplet surface leads to a spatial water concentration gradient with maximum at the droplet center. During the first depletion stage, inner species diffusivity plays an important role in replenishing the evaporated water from the droplet surface by smoothing the concentration gradient. Overestimation of the diffusion coefficients results in an underestimate of the concentration gradient. This leads to an overestimate of the water content at the droplet surface, which leads to an overestimate of the droplet regression rate during the first stage as observed in Figure 3a. Furthermore, the duration of the first stage is expected to be prolonged to vaporize the excess surface water content. Further deviation can be attributed to experimental uncertainties. In particular, Wang et al.[35] experienced ambient temperature fluctuations due to the flow of fresh air at room temperature to the heated chamber. Inevitably, temperature fluctuations decrease the droplet decay rate. Such fluctuations can explain partly the slight overestimation of the numerically predicted droplet decay rate in Figure 3a. Furthermore, Wang et al.[35] stated that the suspended droplet does not maintain its spherical shape while depleting because of gravitational effects and droplet/fiber interactions. Deviations from the purely spherical shape result in an increase in the surface area of the droplet and, consequently, an increase in the evaporation rate. Shape deviation seems to be the main reason behind the underestimation of numerically predicted droplet decay rate in Figure 3b.

Once the droplet surface water content is completely vaporized, the second depletion stage commences, during which the remaining water content vaporizes and urea depletes. The second stage is characterized by a deceleration of the droplet decay rate, followed by a seemingly constant decay rate. The noticeable deviations among the numerical results of the droplet decay rate affirm that the second decomposition stage represents urea depletion because of the variations in the modeling approaches of urea depleting. For the models based on the direct decomposition approach, the rate of urea depletion is directly related to thermolysis activation energy. Hence, for the direct decomposition approach, the descending order of the numerically predicted urea depletion rate should be; (1) Kinetics-V1, (2) Kinetics-V3, (3) Kinetics-V2, and (4) Kinetics-S. Such order is clearly depicted in Figures 3a and 3b. As urea saturation pressure for Vap1 is higher than that for Vap2, the numerical results predicted by Vap1 shows a higher depleting rate of urea. Comparison with experimental data reveals that Vap1 is the most suitable model capable of capturing the experimentally observed depletion behavior quantitatively and qualitatively. The superiority of the results of Vap1 over Vap2 indicates that urea latent heat of vaporization, $L_{vap,u}$, is being underestimated in the Vap2 approach. Such behavior indicates that the correlation for $Cp_{u(g)}$ implemented in Fluent 6.3.2 software[45] is much smaller than the actual one. Rigorous experimental studies are required to accurately measure the properties of gaseous urea. Following the suggestion of Birkhold et al.,[26] the specific heat of urea was modified to represent the specific heat of equimolar mixture of ammonia and isocyanic acid. Such modifications results in an increase of the value of $Cp_{u(g)}$ compared with the one specified in Fluent 6.3.2 software.[45] Although this modifications result in an improvement in the predictability of Vap2, such modifications could not predict superior results to the Vap1 approach.

Further insight into the applicability of the modeling approach can be depicted from the temporal evolution of the droplet surface temperature, which is presented in Figures 4a and 4b for the same conditions in Figures 3a and 3b, respectively. Unfortunately, no experimental data regarding the temperature history of UWS droplet was reported. Figure 4 shows that initially the droplet rapidly heats up to the wet bulb temperature of water. Comparison with Figure 3 shows that no noticeable droplet depletion occurs during the heating period. The droplet maintains its wet bulb temperature over a sustainable portion of the first depletion stage. The decrease of the water content in the droplet surface leads to a decrease in water vaporization rate, which leads to an increase in the droplet surface temperature to maintain the energy balance at the droplet surface as indicated in Eq. 2. The increase in temperature is demonstrated in Figure 4 for both ambient conditions. The rate of temperature elevation rapidly increases due to the rapid decrease in the water content at the droplet surface. Rapid temperature elevation can be referred to as second heating stage, and it is correlated to the decrease in droplet decay rate at the beginning of the second depleting stage. The temperature increases until it reaches urea wet bulb temperature, which varies according to the modeling approach, parameters, and ambient

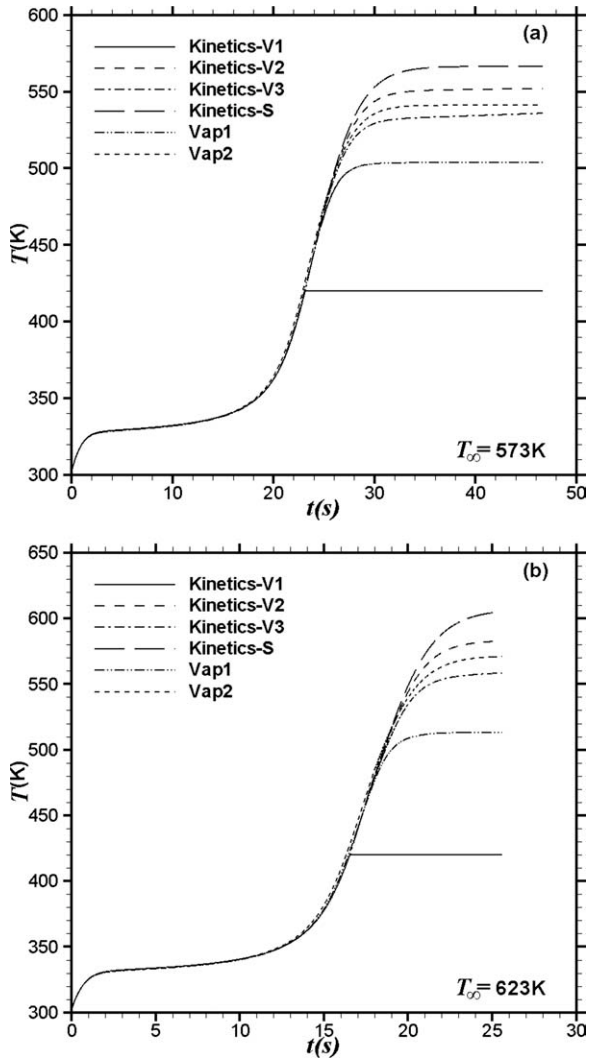

Figure 4. Numerical predictions of the temporal evolution of the surface temperature, T_s, of a UWS droplet size, under the following conditions: (a) T_∞ = 573 K, P_∞ = 1 atm, $Y_{u,\infty} = Y_{w,\infty} = 0$, $T_{l,0}$ = 300 K, d_0 = 0.920 mm, and $Y_{u,0}$ = 0.325; and (b) T_∞ = 623 K, P_∞ = 1 atm, $Y_{u,\infty} = Y_{w,\infty} = 0$, $T_{l,0}$ = 300 K, d_0 = 0.869 mm, and $Y_{u,0}$ = 0.325.

conditions. The striking feature of Figure 4 is that the wet bulb temperature of Kinetics-V1 is 425K, which is the critical temperature for the onset of urea decomposition. Such behavior is unrealistic for the current conditions because the experimental data of Wang et al.[35] demonstrate that solidified deposits remain at the end of droplet depletion period for the conditions in Figures 4a and 4b. Such deposits require the droplet temperature to be higher than 463 K. Given the analysis presented above, it is further confirmed that Vap1 model is the most suitable model to describe urea depletion from UWS droplet.

Internal gasification

One of the most striking features of the experimental data of Wang et al.[35] is the sudden increase of the droplet size at the beginning of the second depleting stage. The entrapment of water inside the droplet due to diffusion resistance was proposed as the reason behind the droplet swelling. During this period, the droplet core temperature can be increased beyond the effective boiling point of water, resulting in water gasification, and consequently size enlargement. The validity of such explanation is explored in the current section.

Figure 5 shows the temporal variations of the mass fractions of water, Y_w and urea, Y_u at the surface and center of the UWS droplet for the same conditions as in Figures 3a and 3b. As expected all models predict the same history of Y_w and Y_u because it is governed by the water vaporization process. The only deviation occurs for Kinetics-V1 near the end of water

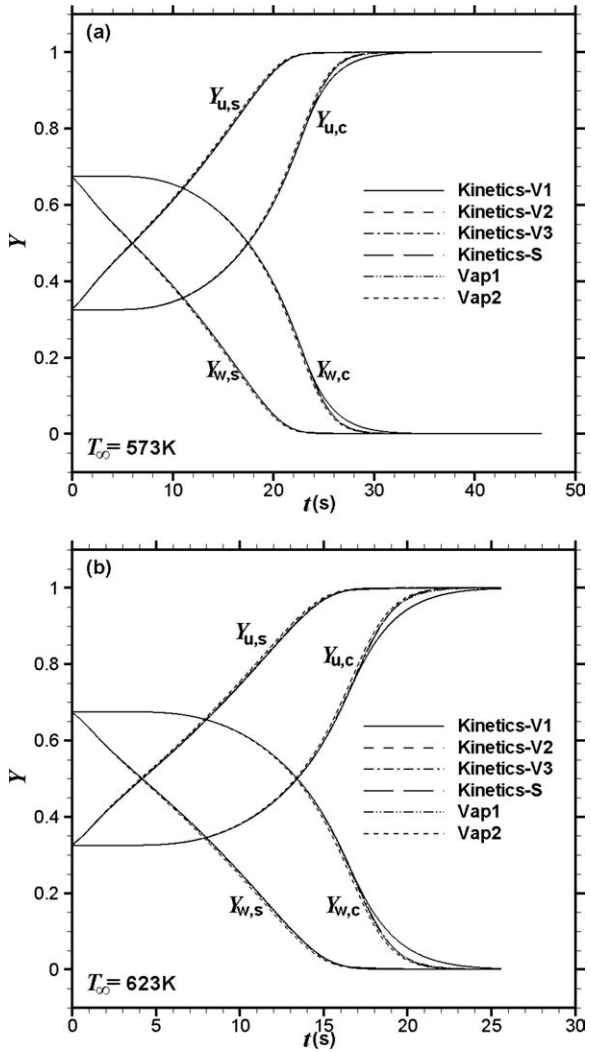

Figure 5. Numerical predictions of the temporal evolution of the species concentration of a UWS droplet size at the droplet surface, $Y_{i,s}$, and center, $Y_{i,c}$, under the following conditions: (a) T_∞ = 573 K, P_∞ = 1 atm, $Y_{u,\infty} = Y_{w,\infty} = 0$, $T_{l,0}$ = 300 K, d_0 = 0.920 mm, and $Y_{u,0}$ = 0.325; and (b) T_∞ = 623 K, P_∞ = 1 atm, $Y_{u,\infty} = Y_{w,\infty} = 0$, $T_{l,0}$ = 300 K, d_0 = 0.869 mm, and $Y_{u,0}$ = 0.325.

presence because of the apparent increase in the urea depleting rate. Regardless of the deviation, a noticeable amount of water is trapped inside the droplet at the beginning of the second decomposition stage. Comparison with Figure 4 shows that the local temperature of the entrapped water is higher than 373 K, which is the boiling temperature of pure water at standard atmospheric conditions. Evident water entrapment triggers the question whether the trapped water reaches the effective boiling point and, consequently, experiences phase transition inside the droplet. As the highest water content is expected to be at the core of the droplet, and the uniform temperature distribution within the droplet during the second depletion stage because of high thermal diffusivity, the critical conditions for the onset of internal gasification should be examined at the center of the droplet. As suggested by Sirignano and Wu,[38] the effective boiling point of entrapped water can be estimated from Raoult's law, such that

$$T_{w(b),c}^{-1} - T_{w(b),\text{pure}}^{-1} = \frac{R \ln X_{w,c}}{L_{\text{vap},w}}. \quad (27)$$

Figure 6 indicates that the effective boiling point of the entrapped water is lower than the droplet center temperature, $T_{l,c}$, for both ambient conditions at the beginning of the second depletion stage. In other words, the droplet center temperature is high enough to cause phase transition of entrapped water. Density differences between liquid and gaseous states cause droplet swelling as experimentally observed by Wang et al.[38] It is interesting to note that apart from Kinetics-V1, all modeling approaches predicted the same gasification period. Such behavior is expected because the droplet temperature reaches urea wet bulb temperature much earlier in the case of Kinetics-V1. Furthermore, the dominator for Kinetics-V1 is considerably smaller than the dominators for other modeling approaches as depicted from Figure 4.

Internal gasification does not necessarily lead to the onset of microexplosion, which is governed by the rates of both nucleation and species diffusion. Figure 5 demonstrates that during the interior gasification region, droplet water content rapidly depletes from the entire droplet composition as indicated by the rapid decay of $Y_{w,c}$. In other words, diffusional transport is significantly improved during the interior gasification region because the droplet size becomes comparable with the characteristic diffusion length.[36] Surface regression due to urea depletion results in exposing more water content at the surface. The exposed water content is expected to rapidly deplete because of its high temperature. In that sense, one can deduce that the nucleation rate is much smaller than the diffusional transport rate, which reduces the occurrence probability of microexplosion. In particular, the experimental results of Wang et al.[35] demonstrated no evidence of disruptive fragmentation of the droplet because its decay rate remains constant during and after the interior gasification period for the conditions examined in the current study.

Proposed decomposition mechanism for UWS droplet

Another interesting phenomenon in the experimentally extracted depletion mechanism is the rapid fluctuation of droplet size during the second depletion stage. Interior gasification of water content cannot be blamed for such fluctuations mainly because hardly any water content remains after the internal gasification period. Furthermore, the cause of the fluctuations seems to emerge from the region close to the droplet surface because the droplet maintains its presence. If the cause emerges from the region near the center, disruptive fragmentation of the droplet would occur. The fluctuation seems to occur due to the fragmentation of the droplet shell only.

To explain the reason behind such fluctuations, one has to correlate the complex mechanism of urea decomposition to the temporal evolution of droplet depletion, temperature, and concentration. Schaber et al.[20] proposed a plausible temperature-dependent reaction scheme for the thermal decomposition of urea in an open reaction vessel using TGA, high-performance liquid chromatography, FTIR, and an ammonium ion-selective electrode. Urea thermal decomposition was divided into four temperature-dependent reaction regimes. The first reaction region extends from room temperature up to 463 K and corresponds to urea vaporization and subsequent decomposition as indicated by reaction (R4). Noticeable mass loss due to urea vaporization starts around 413 K. Significant mass loss seems to result mainly from thermal decomposition, and it starts around 425 K. This is the reason behind selecting 425 K as the critical temperature for the onset of urea depletion according to the direct decomposition approach. Biuret production starts around 433 K due to the reaction of HNCO with the intact urea, such that

$$\mathrm{H_2N{-}CO{-}NH_2}(l) + \mathrm{HNCO(g)} \xrightarrow{\text{heat}} \mathrm{NH_2{-}CO{-}NH{-}CO{-}NH_2}(l), \quad (R6)$$

The second reaction region extends from 463 to 523 K. During this stage, urea decomposition according to (R4) continues, and biuret decomposes into cyanuric acid (CYA), ammelide, and ammeline

$$2\mathrm{NH_2{-}CO{-}NH{-}CO{-}NH_2}(l) \xrightarrow{\text{heat}} \mathrm{CYA}(s) + \mathrm{HNCO}(g) + 2\mathrm{NH_3}(g), \quad (R7)$$

$$2\mathrm{NH_2{-}CO{-}NH{-}CO{-}NH_2}(l) \xrightarrow{\text{heat}} \text{ammelide}(s) + \mathrm{HNCO}(g) + \mathrm{NH_3}(g) + \mathrm{H_2O}(g), \quad (R8)$$

$$\mathrm{NH_2{-}CO{-}NH{-}CO{-}NH_2}(l) + \mathrm{HNCO}(g) \xrightarrow{\text{heat}} \text{ammeline}(s) + 2\mathrm{H_2O}(g), \quad (R9)$$

The remaining solid mass at the end of the second reaction regime is mainly composed of CYA and ammelide with 2:1 molar ratio. The remaining solids are expected to be thermally stable during the third reaction regime, which extends from 523 to 633 K. Heating the sample above 633 K, which corresponds to the fourth reaction regime, will result in the rapid decay of the remaining solid mass through sublimation and decomposition.

The numerical results presented in Figure 4 demonstrate that the droplet wet bulb temperature for Vap1 is higher than the critical temperatures for biuret formation of 433 K and decomposition of 463 K. Furthermore, urea mass fraction at the surface is almost unity during the second depletion stage. The high mass fraction of urea and surface

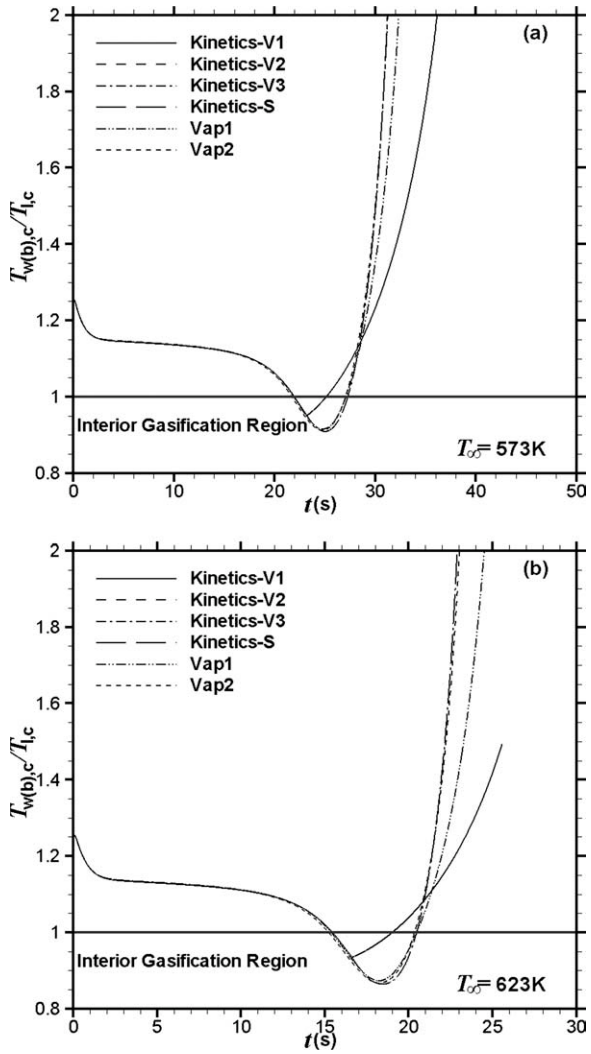

Figure 6. Numerical predictions of the temporal variations of the trapped water effective boiling temperature, $T_{b,loc}$, with respect to the droplet center temperature, $T_{l,c}$, under the following conditions: (a) T_∞ = 573 K, P_∞ = 1 atm, $Y_{u,\infty} = Y_{w,\infty} = 0$, $T_{l,0}$ = 300 K, d_0 = 0.920 mm, and $Y_{u,0}$ = 0.325; and (b) T_∞ = 623 K, P_∞ = 1 atm, $Y_{u,\infty} = Y_{w,\infty} = 0$, $T_{l,0}$ = 300 K, d_0 = 0.869 mm, and $Y_{u,0}$ = 0.325.

The interior gasification region is highlighted.

temperature combined with the absence of convection in the quiescent environment compose an ideal situation for biuret formation according to reaction (R6). The formed biuret readily decompose into the solid components of CYA, ammelide, and ammeline according to reactions (R7)–(R9). These solid components form a shell around the molten urea. The entrapped urea vaporizes and readily decomposes into gaseous ammonia and isocyanic acid according to reaction (R4). The rapid gasification of urea near the solid shell results in a sudden swelling of the droplet. Pressure buildup due to urea gasification causes the thin shell to shatter and, consequently, a reduction in the droplet size. This mechanism will be repeated until the interior pressure buildup is not large enough to crack the solid shell. In this case, more urea will be transformed into biuret, which will rapidly decompose into the solid deposits. The shell thickness will consequently increase until it occupies the whole droplet. The solidified deposits were observed experimentally by Wang et al.[35]

Comparison between DL and RM approaches

In a typical urea-based SCR system, UWS is introduced as a spray composed of thousands of droplet parcels. The implementation of the DL approach is computationally too costly. The RM approach is an attractive alternative due to the elimination of the discretization of the droplet interior. However, the question regarding the reliability of the simplified RM approach to represent the decay mechanism of UWS droplet arises. Answering this question requires direct comparison between the predictions of RM and DL. Ambient and droplet initial conditions should represent the exhaust pipe conditions, and the SMD of the UWS spray injected in practical urea-based SCR systems. The exhaust pipe operates near atmospheric pressure conditions, and the temperature range varies between 400–1000 K. The practical range of SMD varies from 20–150 μm. It should be noted that the practical SMD is about 10 times smaller than the initial droplet size implemented in the experimental study of Wang et al.[35]

Figure 7 shows the temporal variations of the diameter and surface temperature of a typical UWS droplet using both RM and DL approaches, and Vap2 for urea depletion. Although the results presented in Figure 3 shows the superiority of Vap1 approach, Vap2 approach is physically more appropriate because it incorporates the thermal variations of $L_{vap,u}$. Implementing accurately measured $Cp_{u,g}$ in Vap2 approach will ultimately improve the predictability of Vap2 over Vap1. The ambient and initial droplet conditions are T_∞ = 573 K, P_∞ = 1 atm, $Y_{u,\infty} = Y_{w,\infty} = 0$, $T_{l,0}$ = 300 K, d_0 = 70 μm, and $Y_{u,0}$ = 0.325 in Figure 7a and T_∞ = 673 K, P_∞ = 1 atm, $Y_{u,\infty} = Y_{w,\infty} = 0$, $T_{l,0}$ = 300 K, d_0 = 70 μm, and $Y_{u,0}$ = 0.325 in Figure 7b. As depicted from Figure 8, both RM and DL approaches show the same qualitative behavior. Noticeable deviations between the RM and DL approaches occur in the wet bulb temperature of water and the droplet depletion rate during the second heating period. The deviations between these two approaches can be explained by correlating Figures 7 and 8, which show the temporal variations of species concentrations.

The RM approach is a limiting case postulating infinitely high diffusivities for the liquid phase. In that sense, surface water depleting mass becomes replenished at an infinitely high rate to smooth out the concentration gradient within the droplet. Hence, the RM approach predicts higher water content at the droplet surface as clearly illustrated in Figure 8. This will lead to a higher evaporation rate as shown in Figures 7a and 7b. The increase in the evaporation rate results in a lower wet bulb temperature as required by the energy balance. Figure 7 shows that the wet bulb temperature of the RM approach is slightly lower than that of the DL approach for both ambient conditions. Furthermore, the duration of the water vaporization stage is expected to be prolonged for the RM approach to vaporize the excess

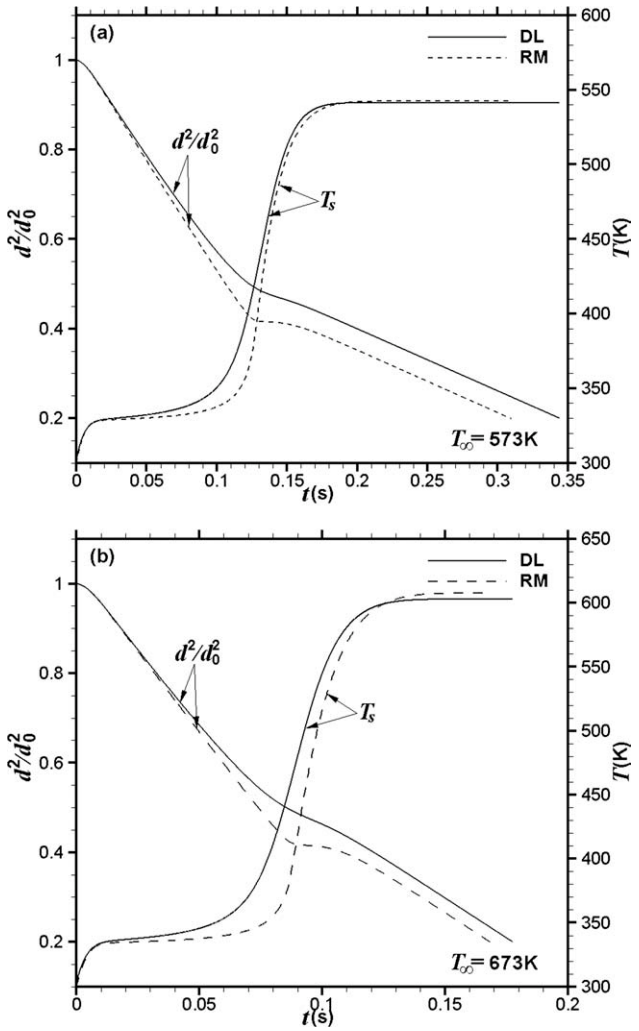

Figure 7. Comparison between the numerical results of the diffusion limit (DL) and rapid mixing (RM) approaches for the time evolution of the surface temperature, T_s, and size, d^2/d_0^2, of a UWS droplet.

The ambient and initial conditions are: (**a**) $T_\infty = 573$ K, $P_\infty = 1$ atm, $Y_{u,\infty} = Y_{w,\infty} = 0$, $T_{l,0} = 300$ K, $d_0 = 70$ μm, $Y_{u,0} = 0.325$; and (**b**) $T_\infty = 673$ K, $P_\infty = 1$ atm, $Y_{u,\infty} = Y_{w,\infty} = 0$, $T_{l,0} = 300$ K, $d_0 = 70$ μm, $Y_{u,0} = 0.325$.

surface water content as illustrated in Figures 7a and 7b. During the second heating stage, the droplet water content is much smaller for the RM approach as depicted from Figures 8a and 8b. Hence, the droplet depletion rate is smaller for the RM approach during the second heating stage. In fact, Figure 7 shows that the droplet depletion rate almost vanishes during the second heating stage for the RM model. Some water content is expected to be entrapped for the DL approach because of the finite value of diffusivity. Consequently, urea wet bulb temperature predicted by the DL approach is lower than the one predicted by the RM approach, as demonstrated in Figures 7a and 7b. It is interesting to note that the difference between the RM and DL predictions of wet bulb temperature is higher for the conditions in Figure 7b. This is due to the excess energy in the higher temperature region, which results in a larger heating rate and, consequently, more water entrapment.

For design purposes, the important parameters are the urea depletion rate and the required duration for complete droplet depletion. Figure 7 shows that the RM approach overestimates the droplet depletion rate and, consequently, underestimates the depletion duration. Although the droplet duration was underestimated by 10% for the conditions in Figure 7a, it was underestimated by only 5% for the conditions in Figure 7b. In that sense, the deviations among RM and DL vary according to the operating conditions. It seems that the higher the ambient temperature, the lower the deviation. The influence of the initial droplet size on the depleting duration,

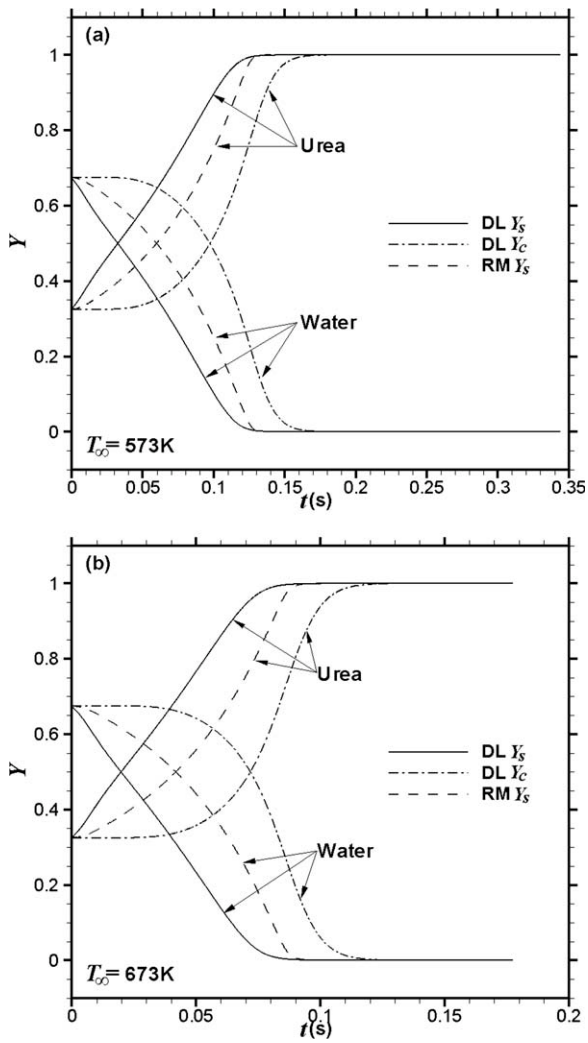

Figure 8. Comparison between the numerical results of DL and RM approaches for the time evolution of the species concentration of a UWS droplet size at the droplet surface, $Y_{i,s}$, and center, $Y_{i,c}$.

The ambient and initial conditions are: (**a**) $T_\infty = 573$ K, $P_\infty = 1$ atm, $Y_{u,\infty} = Y_{w,\infty} = 0$, $T_{l,0} = 300$ K, $d_0 = 70$ μm, $Y_{u,0} = 0.325$; and (**b**) $T_\infty = 673$ K, $P_\infty = 1$ atm, $Y_{u,\infty} = Y_{w,\infty} = 0$, $T_{l,0} = 300$ K, $d_0 = 70$ μm, $Y_{u,0} = 0.325$.

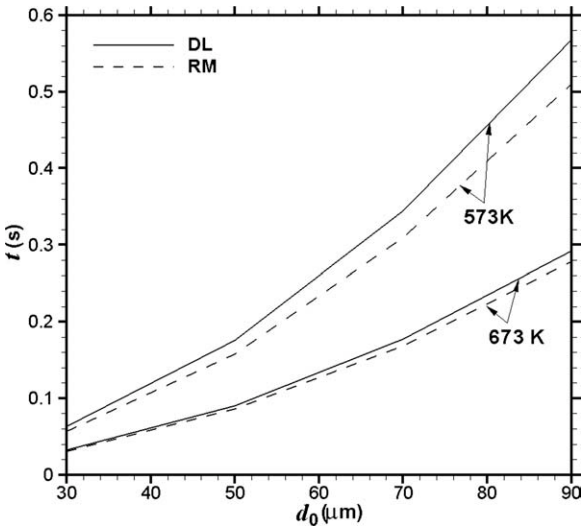

Figure 9. Comparison between the numerical results of DL and RM approaches for the variation of the duration of UWS droplet depletion with droplet initial diameter, d_0, under two different ambient conditions, namely; (i) T_∞ = 573 K, P_∞ = 1 atm and (ii) T_∞ = 673 K, P_∞ = 1 atm.

The droplets initial conditions are $Y_{u,\infty} = Y_{w,\infty} = 0$ and $T_{l,0}$= 300 K.

as shown in Figure 9, indicates that an increase in the initial droplet size results in a slight increase in the deviation between RM and DL approach. This is expected because diffusivity effects become more pronounced as the droplet size increases. Such small deviation is encouraging to apply the RM approach for spray modeling.

Conclusions

Two theoretical models describing the depleting process of a typical UWS droplet in a heated environment as experienced in an automotive urea-based automotive SCR system are proposed and implemented in the current study. In accordance with experimental data, both theoretical models show that the depletion of UWS droplet in heated environment can be divided into two stages; water vaporization followed by urea depletion. Comparison with the experimental data of the decay rate of an individual UWS, droplet in heated environment reveals the superiority of modeling urea depleting process as a vaporization process. Because of diffusion resistance, the entrapment of water inside the droplet at the beginning of urea depletion stage is demonstrated. Hence, at the beginning of urea depletion stage, the UWS droplet should be represented as a highly concentrated urea droplet rather than a pure urea droplet for better estimate of the temporal evolution of droplet size and temperature. The effective local boiling point of entrapped water is calculated to be higher than 373 K. The critical conditions for the onset of droplet swelling due to internal gasification of entrapped water are identified. Although internal gasification will occur for the conditions examined in the current study, it will not lead to microexplosion because of the relatively small water content and the rapid depletion rate of water. The experimentally observed fluctuations in the droplet decay rate in the quiescent environment are found to be due to the formation and fragmentation of solid complexes at the droplet surface. Finally, the current study demonstrates the suitability of implementing the RM approach to model the depletion process of UWS through comparison with the results of DL approach at various operating conditions.

Acknowledgments

The financial support from the Ontario Research Fund-Research Excellence (ORF-RE) program via contract # RE-02-019 is greatly appreciated.

Notation

A = pre-exponential factor (1/s) or (kg/m s)
B_M = global mass transfer number
B_T = global heat transfer number
C_p = specific heat (J/Kg K)
D = droplet diameter (m)
E = activation energy (J/mol)
F_M, F_T = correction factors
h = heat transfer coefficient (W/m^{2}K)
h_m = mass transfer coefficient (m/s)
H = molar enthalpy of reaction (J/kg)
j = mass diffusion rate (kg/s)
K = thermal conductivity (W/m K)
L_{vap} = latent heat of vaporization (J/kg)
m = mass (kg)
MW = molecular weight (kg/kmol)
Nu = Nusselt number
P = pressure (Pa)
Pr = Prandtl number
$\dot{Q}$ = heat-transfer rate (W)
r = radial location
R = universal gas constant (J/mol K)
Re_l = droplet Reynolds number
$Sc_{i,g}$ = Schmidt number
Sh = Sherwood number
t = time (s)
T = temperature (K)
v = velocity (m/s)
X = mole fraction
Y = mass fraction

Greek letters

α = thermal diffusivity (m^2/s)
ε = emissivity
ν = dynamic viscosity (m^2/s)
ρ = density (kg/m^3)
σ = Stefan–Boltzmann constant (5.67×10^{-8} W/m^2 K)
Γ = mass diffusion coefficient (m^2/s)

Subscripts

0 = initial condition
∞ = ambient
B = boiling point
c = center
g = gas phase
i = species index
l = liquid phase
rad = radiation
rel = relative
s = surface
sat = saturation
std = standard conditions (T = 298 K and P = 1 atm)
th = thermolysis

u = urea
w = water
wall = exhaust wall

Other notations

$\bar{}$ = spatial average
$\dot{}$ = temporal rate of change
$[i]$ = molar concentration of species i (kmol/m^3)

Literature Cited

1. Flynn PF, Durrett RP, Hunter GL, Akinemi WC, Farrell LA. Minimum engine flame temperature impacts on diesel and spark-ignition engine NOx production. In *Proceedings of SAE World Congress*. Detroit, MI, 2000, SAE Paper 2000-01-1177.
2. Sharp CA, Howell SA, Jobe J. The effect of biodiesel fuels on transient emissions from modern diesel engines, Part I: Regulated emissions and performance. In Proceedings of SAE Spring Fuels and Lubricants Meeting and Exposition. Paris, France, 2000, SAE Paper 2000-01-1967.
3. United States Environmental Protection Agency. A comprehensive analysis of biodiesel impact on exhaust emissions. Draft Technical Report EPA420-P-02–001, 2002.
4. Kröcher O, Elsener M, Jacob E. A model gas study of ammonium format as alternative ammonia precursor compounds for the selective catalytic reduction of nitrogen oxides in diesel exhaust gas. *Appl Catal B-Environ*. 2009;88:66–82.
5. Heywood JB. *Internal Combustion Engine Fundamentals*. New York: McGraw, 1988.
6. Hoard J. Plasma-catalysis for diesel exhaust treatment: current state of the art. *SAE Trans*. 2001;110:2001-01-0185.
7. Johnson TV. Review of diesel emissions and control. *SAE Int J Fuel Lubr*. 2010;3:16–29.
8. Twigg MV. Progress and future challenges in controlling automotive exhaust gas emissions. *Appl Catal B Environ*. 2007;70:2–15.
9. Koebel M, Elsener M, Kleemann M, Urea-SCR: a promising technique to reduce NOx emissions from automotive diesel engines. *Catal Today*. 2000;59:335–345.
10. Cooper BJ, McDonald AC, Walker AP, Sanchez M. The development and on-road performance and durability of the four-way emission control SCRT system. 2003 US Department of Energy Emission Reduction (DEER) Conference. Newport, RI, 2003.
11. Johnson TV. Diesel emission control in review. *SAE Int J Fuel Lubr*. 2008;1:68–81.
12. ACEA Report on Selective Catalytic Reduction. The most promising technology to comply with imminent Euro IV and Euro V emissions standards for HD engines. 2003.
13. Kleemann M, Elsener M, Koebel M, Wakaun A. Hydrolysis of isocyanic acid on SCR catalysts. *Ind Eng Chem Res*. 2000;39:4120–4126.
14. Gabrielsson PLT. Urea-SCR in automotive applications. *Top Catal*. 2004;28:177–184.
15. Elvers B. *Ullmann's Encyclopedia of Industrial Chemistry*, 5th ed. Weinheim: VCH; 1985;A27:358–365.
16. Oesterle JJ, Calvo S, Damson B, Neuman F, Rudelt J. SCR technology with focus to stringent emissions legislation. In *Proceedings of SAE International Commercial Vehicle Engineering Congress and Exhibition*. Rosemont, IL, 2008, SAE Paper 2008-01-2640.
17. Koebel M, Elsener M, Madia G. Recent advances in the development of urea-SCR for automotive applications. In Proceedings of SAE International Fall Fuels and Lubricants Meeting & Exhibition. San Antonio, TX, 2001, SAE Paper 2001-01-3625.
18. Yim SD, Kim SJ, Baik JH, Nam I, Mok YS, Lee JH, Cho B, Oh SH. Decomposition of urea into NH3 for the SCR process. *Ind Eng Chem Res*. 2004;43:4856–4863.
19. Fang HL, DaCosta HFM. Urea thermolysis and NOx reduction with and without SCR catalyst. *Appl Catal B Environ*. 2003;46:17–34.
20. Schaber OM, Colson J, Higgins S, Thielen D, Anspach B, Brauer J. Thermal decomposition (pyrolysis) of urea in an open reaction vessel. *Thermochim Acta*. 2004;424:131–142.
21. Ström H, Lundström A, Andersson B. Choice of urea-spray models in CFD simulations of urea-SCR systems. *Chem Eng J*. 2009;150:69–82.
22. Chi JN, DaCosta HFM. Modeling and control of a urea-SCR aftertreatment system. In *Proceedings of SAE World Congress*. Detroit, MI, 2005, SAE Paper 2005-01-0966.
23. Chen M, William S. Modeling and optimization of SCR-exhaust aftertreatment systems. In *Proceedings of SAE World Congress*. Detroit, MI, 2005, SAE Paper 2005-01-0969.
24. Kim JY, Ryu SH, Ha JS. Numerical predictions on the characteristics of spray-induced mixing and thermal decomposition of urea solution in SCR System. In *Proceedings of 2004 Fall Technical Conference of the ASME Internal Combustion Engine Division*, Long Beach, CA, 2004; 165–170.
25. Birkhold F, Meingast U, Wassermann P, Deutschmann O. Analysis of the injection of urea-water-solution for automotive SCR DeNOx-systems: Modeling of two-phase flow and spray/wall-interaction. In *Proceedings of SAE World Congress*. Detroit, MI, 2006, SAE Paper 2006-01-0643.
26. Birkhold F, Meingast U, Wassermann P, Deutschmann O. Modeling and simulation of the injection of urea-water-solution for automotive SCR DeNOx-systems. *Appl Catal B Environ*. 2007;70:119–127.
27. Yi Y. *Development of a 3D numerical model for predicting spray, urea decomposition and mixing in SCR systems*. In *Proceedings of SAE World Congress*. Detroit, MI, 2006, SAE Paper 2007-01-3985.
28. Munnannur A, Liu ZG. *A multi-dimensional model for DEF injection and urea decompose-tion in mobile SCR DeNOx systems*. In *Proceedings of 4th Biennial Conf. Addressing Today's Challenges and Future Needs: Emission Solutions in Transportation*. Ann Arbor, MI, 2009.
29. Munnannur A, Liu ZG. *Development and validation of a predictive model for DEF injection and urea decomposition in mobile SCR DeNOx systems*. In *Proceedings of SAE World Congress*. Detroit, MI, 2010, SAE Paper 2010-01-0889.
30. Abramzon B, Sirgnano WA. Droplet vaporization model for spray combustion calculations. *Int J Heat Mass Transfer*. 1989;32:1605–1618.
31. Renksizbulut M, Yuen MC. Numerical study of droplet evaporation in a high-temperature stream. *J Heat Transfer*. 1983;105:389–397.
32. Lundström A, Andersson B, Olsson L. Urea thermolysis studied under flow reactor conditions using DSC and FT-IR. *Chem Eng J*. 2009;150:544–550.
33. Emel'yanenko VN, Kabo GJ, Verevkin SP. Measurement and prediction of thermochemical properties: improved increments for the estimation of enthalpies of sublimation and standard enthalpies of formation of alkyl derivatives of urea. *J Chem Eng Data*. 2006;51:79–87.
34. Abu-Ramadan E, Li X. Recent advances and future challenges in the modeling and simulation of the injection of urea-water- solution for automotive SCR systems. Directions in Energy-Efficiency and Emissions Research Conference (DEER). Dearborn, MI, 2009.
35. Wang TJ, Baek SW, Lee SY, Kang DH, Yeo GK. Experimental investigation on evaporation of urea-water-solution droplet for SCR applications. *AIChE J*. 2009;55:3267–3276.
36. Law CK. Internal boiling and superheating in vaporizing multicomponent droplets. *AIChE J*. 1978;24:626–632.
37. Wang CH, Liu XQ, Law CK. Combustion and microexplosion of freely falling multicomponent droplets. *Combust Flame*. 1984;56:175–197.
38. Sirgnano WA, Wu G. Multicomponent-liquid-fuel vaporization with complex configuration. *Int J Heat Mass Transfer*. 2008;51:4759–4774.
39. Renksizbulut M, Bussmann M, Li X. A droplet vaporization model for spray calculations. *Part Part Syst Charact*. 1992;9:59–95.
40. Raznjevic K. *Handbook of Thermodynamic Tables and Charts*. New York: McGraw; 1976.
41. Clift R, Grace JR, Weber ME. *Bubbles, Drops, and Particles*. New York: Academic Press; 1978.
42. Renksizbulut M, Yuen MC. Experimental study of droplet evaporation in a high-temperature air stream. *J Heat Transfer*. 1983;105:384–388.
43. Badzioch S, Hawksley PG. Kinetics of thermal decomposition of pulverized coal particles. *Ind Eng Chem Proc DD*. 1970;9:521–530.

44. Poling BE, Prauznitz JM. O'Connell JP. *The Properties of Gaseous and Liquids*, 5th ed. New York: McGraw-Hill; 2001.
45. FLUENT 6.3.2 Software. Fluent Inc., Lebanon, NH, 2006.
46. Gmelin Handbook of Inorganic and Organometallic Chemistry. Editor-in-chief: Gmelin Institute for Inorganic Chemistry of the Max-Planck-Society for Advancement of Science. Berlin: Springer; 1997; C: MVol.D1, 45.5.2: 410-411.
47. *AdBlue, Technical Leaflet. BASF Aktiengesellschaft*, Ludwigshafen, Germany, Feb. 2005.
48. Longsworth LG. Temperature dependence of diffusion in aqueous solutions. *J Phys Chem*. 1954;58:770–773.
49. Aoki H, Fujiwara T, Morozumi YE, Miura T. Measuremetns of urea thermal decomposition reaction for NO selective non-catalytic reduction. In *Proceedings of 5th International Conference on Technologies and Combustion for a Clean Environment*, Lisbon, Portugal; 1999:115–118.
50. Daif A, Bouaziz M, Chesneau X, Ali Chérif A. Comparison of multicomponent fuel droplet vaporization experiments in forced convection with the Sirignano model. *Exp Therm Fluid Sci*. 1999;18:282–2910.

Appendix: Nondimensional Governing Equations

Energy equation for the droplet:

$$\bar{r}_s^2 \frac{\partial \bar{T}}{\partial \tau} - 0.5 \frac{d\bar{r}_s^2}{d\tau} \eta \frac{\partial \bar{T}}{\partial \eta} = \frac{X_t}{\eta^2} \frac{\partial}{\partial \eta} \left(\eta^2 \frac{\partial \bar{T}}{\partial \eta} \right) \tag{A1}$$

Species equation for the droplet:

$$Le_L \bar{r}_s^2 \frac{\partial \bar{\chi}}{\partial \tau} - 0.5 Le_L \frac{d\bar{r}_s^2}{d\tau} \eta \frac{\partial \bar{\chi}}{\partial \eta} = \frac{X_d}{\eta^2} \frac{\partial}{\partial \eta} \left(\eta^2 \frac{\partial \bar{\chi}}{\partial \eta} \right) \tag{A2}$$

where $\bar{r}_s = r_s/r_o$, $\tau = \alpha_l t/r_o^2$, $\eta = r/r_s$, $\bar{\chi} = (\chi - \chi_o)/\chi_o$, $\overline{T} = (T - T_o)/T_o$, r_o, and T_o are the initial radius and temperature. α_l is the liquid thermal diffusivity, Le_L is the liquid phase Lewis Number, χ is the solute mass fraction, and r_s is the instantaneous radius.

Manuscript received Sept. 9, 2010, and revision received Nov. 25, 2010.